Mechanical Systems and Signal Processing 131 (2019) 633–648

Contents lists available at ScienceDirect

Mechanical Systems and Signal Processing

journal homepage: www.elsevier.com/locate/ymssp

Local damage detection of membranes based on Bayesian operational modal analysis and three-dimensional digital image correlation

Yujia Hu [a], Weigong Guo [a], Weidong Zhu [b,*], Yongfeng Xu [c]

[a] School of Mechanical Engineering, University of Shanghai for Science and Technology, Shanghai 200093, China
[b] Department of Mechanical Engineering, University of Maryland, Baltimore County, 1000 Hilltop Circle, Baltimore, MD 21250, USA
[c] Department of Mechanical and Materials Engineering, University of Cincinnati, 2600 Clifton Avenue, Cincinnati, OH 45221, USA

ARTICLE INFO

Article history:
Received 1 November 2018
Received in revised form 7 March 2019
Accepted 24 April 2019
Available online 17 June 2019

Keywords:
Damage detection
Bayesian operational modal analysis
Digital image correlation
Membrane

ABSTRACT

It is difficult to detect local damage of a structure based on modal analysis. This paper presents a novel local damage detection method of membranes under ambient excitation, which combines Bayesian operational modal analysis (BOMA) and three-dimensional digital image correlation (3D-DIC). It is a noncontact and full-field dynamic method with no sensors attached on a test membrane. Advantages of BOMA and 3D-DIC methods are integrated in this work. Anomalies caused by local damage in mode shapes and curvature mode shapes can be explicitly observed. Moreover, a mode shape damage index (MSDI) is used to improve local damage detection, and structural damage can be identified in neighborhoods with high values of MSDIs. The methodology is applied, as a demonstration, to detect damage introduced by razor cuts in circular and rectangular membranes with different boundary conditions.

1. Introduction

Using modal analysis for structural damage detection has been a focus of much research in recent years due to its nondestructive and low-cost nature. When damage occurs in a structure, its dynamic stiffness decreases and its modal properties such as natural frequencies, mode shapes, and damping ratios change too. When modal properties are judiciously chosen, some of their changes can be used to identify changes in the structure itself that show if damage exists and its location if it does.

Cawley and Adams [1] used natural frequency shifts to locate and quantity damage. While natural frequency-based methods are able to detect damage, it is difficult to locate the damage location and their sensitivity to damage is not high. More effective methods based on mode shapes and their derivatives have been proposed. Pandey et al. [2] found that changes in curvature mode shapes are localized in the damage area and used the curvature mode shapes to detect damage in a structure. They also noted that changes in the curvature mode shapes increase with the damage size. Ratcliffe [3] localized damage by applying a finite difference approximation of Laplace differential operator to mode shapes without a priori knowledge of an undamaged structure. Stubbs et al. [4] introduced a damage index method based on a modal strain energy using undamaged and damaged structural models. An effective model updating approach was recently proposed for damage

* Corresponding author.
E-mail address: wzhu@umbc.edu (W. Zhu).

https://doi.org/10.1016/j.ymssp.2019.04.051
0888-3270/

detection of buildings and bridges under ambient excitation [5–7]. Such a method used identified modal parameters of a structure (i.e., natural frequencies and mode shapes) to update structural parameters, and identified structural damage from the update model.

However, the traditional method for vibration measurement is to attach sensors on a test structure. Local damage cannot be accurately detected due to a limited number of sensors used in an experiment. The mass added to a lightweight structure such as a membrane by a contact sensor (e.g., an accelerometer) can significantly affect dynamic properties of the structure. It is difficult to obtain modal parameters of membranes by conventional contact test methods. Thus, a noncontact and full-field dynamic method can be well suited for detecting local damage of membranes.

There exist a number of noncontact, full-field, and remote sensing methods for mode shape measurement, such as holographic interferometry [8], laser speckle interferometry [9], and laser speckle photography [10]. Keene and Chiang [11] developed a simple technique to visualize anti-nodes of a vibrating distributed-parameter system in real time using defocused laser speckle contrast analysis and detected damage of membranes. While the technique gives anti-nodes of a structure in real time, it does not provide quantitative information on the amplitude of vibration of the structure. In addition, damage detection in Ref. [11] requires examination of all the images.

Digital image correlation (DIC) has been widely used to measure displacements, strains, and stresses of structures in experimental mechanics [12–15]. Machado et al. [16] obtained stress-strain fields of a membrane using its curvature based on three-dimensional (3D) DIC (3D-DIC) data. While DIC methods are mainly utilized for displacement and strain measurement and determination of material properties, some works have been devoted to vibration analysis. Helfrick et al. [17] provided validation of a 3D-DIC method for full-field vibration measurement. Experimental results from the 3D-DIC method and experimental modal analysis (EMA) were well correlated with results from finite element analysis and those from a scanning laser Doppler vibrometer (SLDV). Reu et al. [18] compared the DIC method and laser Doppler vibrometry in modal measurement. They noted that these two methods can both be used for extracting modal parameters; in general, a 3D-DIC system is much cheaper than a SLDV. Some other researchers also used the 3D-DIC method with EMA to obtain dynamic characteristics of a structure [19–21]. Due to difficulty in recording input excitation data when testing structures are membranes or large-scale structures, operational modal analysis (OMA) instead of EMA can be used in 3D-DIC vibration measurement to evaluate modal properties of a structure with unknown excitation. One primary advantage of OMA is that only output vibration of a structure needs to be measured. Poozesh et al. [22] extracted operational mode shapes of turbine blades using a multi-camera stereo DIC system that is composed of two pairs of synchronized stereo cameras. They used a single input force so that the cross spectrum matrix was measured relative to a particular reference point on the structure. By this way, cross spectra can be used in OMA to obtain operational mode shapes. Poozesh et al. [23] subsequently developed a hybrid output-only system identification method to more accurately extract modal parameters from DIC data.

Since DIC measurement has some limitations in modal analysis with a low sampling rate and short recording-data length due to limitations of cameras, Bayesian OMA (BOMA) is well suited to do modal analysis to overcome these difficulties. A number of BOMA methods have been developed in the last two decades [24–27] with some applications in civil engineering [28–30]. BOMA adopts a Bayesian system identification approach for OMA. Such a method values the traditional fast Fourier transform (FFT) theory as a core and views modal identification as an inference problem in which probability is used as a measure of relative plausibility of outcomes given a model of a structure and measured data central to Bayesian theorem. In particular, BOMA methods are capable of extracting all the information from ambient excitation history data through its posterior statistics and the description method by probability logic better satisfies properties of modal parameters under random excitation. Moreover, it is much more convenient to use BOMA than EMA and conventional OMA methods due to the following reasons: (1) It can extract modal parameters based on only response measurement and it can process response histories at all measured degrees of freedom (DOFs). Only one set of response time histories is required [24]. (2) It can overcome challenges of noisy measurement data and short-length recording data from DIC measurement [25,26]. (3) It obtains not only optimal values of modal parameters, but also uncertainties and signal-to-noise ratios that can be used to evaluate analysis results [26,27].

From the above-mentioned methods with 3D-DIC and BOMA, one can find that: (1) Using 3D-DIC, one can obtain more vibration data compared with the traditional pointwise measurement method, and no mass loading of sensors is added on a test structure. Advantages of 3D-DIC, which are full-field noncontact measurement, bring possibilities for detecting local damage in a structure based on dynamic measurement. (2) Using BOMA for modal parameter identification, one can resolve drawbacks that input excitation data need to be recorded and post-processed in normal 3D-DIC dynamic measurement, such as EMA. BOMA is well suited for modal analysis of membranes and large-scale structures under ambient excitation.

In this work, a novel noncontact, full-field, and remote sensing method that combines BOMA and 3D-DIC is proposed to detect local damage in membranes under ambient excitation. Advantages of BOMA and 3D-DIC are integrated. Modal parameters of structures with local damage are obtained for the first time under ambient excitation. Anomalies caused by local damage in their mode shapes and curvature mode shapes can be explicitly observed. As a demonstration, mode shapes and curvature mode shapes of circular and rectangular membranes with razor cuts and different boundary conditions are successfully used for local damage detection. The method proposed in this paper can provide quantitative information on the amplitude of vibration of a structure and overcome disadvantages of the technique in Ref. [11]. Furthermore, a mode shape damage index (MSDI) in Ref. [31] is used to assist local damage detection, and structural damage can be identified in neighborhoods with high values of MSDIs.

2. Background of the theoretical framework

2.1. BOMA

Yuen et al. [24,25] developed an approach for modal parameter identification using Bayesian FFT of ambient excitation data. Au [26,27] further developed this approach with separated modes that are independently identified. The theory of this methodology is briefly introduced below.

Let $\boldsymbol{\theta}$ be modal parameters of a structure, including the natural frequency f, modal damping ratio ζ, mode shape $\boldsymbol{\Phi}$, power spectral density (PSD) of the modal force S, and PSD of prediction error S_e. Let $\{\hat{\boldsymbol{x}}_j \in \mathbb{R}^n : j = 1, ..., N\}$, where N is the number of samples of a channel of a measurement device, be displacement time histories measured from an n DOF structure. The FFT of $\{\hat{\boldsymbol{x}}_j(t)\}$ is calculated as

$$\mathscr{F}_k = \boldsymbol{F}_k + \mathrm{i}\boldsymbol{G}_k = \sqrt{\frac{2\Delta t}{N}} \sum_{j=1}^{N} \hat{\boldsymbol{x}}_j \exp\left[-2\pi \mathrm{i} \frac{(k-1)(j-1)}{N}\right] \quad (k = 1, \cdots, N) \tag{1}$$

where $\mathrm{i}^2 = -1$, $\mathbf{F}_k$ and $\mathbf{G}_k$ denote real and imaginary parts of the FFT, respectively, Δt is the sampling time step, and $N_q = \mathrm{int}\left[\frac{N}{2}\right] + 1$ denotes the FFT value at Nyquist frequency. For $k = 2, 3 \cdots N_q$, the FFT value corresponds to the frequency $f_k = (k-1)/(N\Delta t)$.

Let $\{\boldsymbol{Z}_k\} = \left[\boldsymbol{F}_k^T, \boldsymbol{G}_k^T\right]^T \in R^{2n}$ be an augmented vector of real and imaginary parts of the FFT. With a large amount of data, $\boldsymbol{Z}_k$ follows a Gaussian distribution with zero mean and its covariance matrix is

$$\boldsymbol{C}_k = \frac{1}{2}\begin{bmatrix} \boldsymbol{\Phi}\mathrm{Re}\boldsymbol{H}_k\boldsymbol{\Phi}^T & -\boldsymbol{\Phi}\mathrm{Im}\boldsymbol{H}_k\boldsymbol{\Phi}^T \\ \boldsymbol{\Phi}\mathrm{Im}\boldsymbol{H}_k\boldsymbol{\Phi}^T & \boldsymbol{\Phi}\mathrm{Re}\boldsymbol{H}_k\boldsymbol{\Phi}^T \end{bmatrix} + \frac{S_e}{2}\boldsymbol{I}_{2n} \tag{2}$$

where Re and Im denote real and imaginary parts of a complex variable, respective, $\boldsymbol{\Phi} = [\boldsymbol{\Phi}_1, \cdots, \boldsymbol{\Phi}_m] \in R^{n\times m}$ is the mode shape matrix, $\boldsymbol{I}_{2n} \in R^{2n\times 2n}$ is an identity matrix, and $\boldsymbol{H}_k$ is the spectral density matrix of modal response with its (i,j) element given by

$$\boldsymbol{H}_k(i,j) = S_{ij} f_k^{-4}\left[(\beta_{ik}^2 - 1) + \mathrm{i}(2\zeta_i\beta_{ik})\right]^{-1}\left[(\beta_{jk}^2 - 1) - \mathrm{i}(2\zeta_j\beta_{jk})\right]^{-1} \tag{3}$$

with $\beta_{ik} = f_i/f_k$, in which f_i and ζ_i are the natural frequency and damping ratio of the i th mode, respectively, and S_{ij} is the cross spectral density between the i th and j th modal excitation.

In Bayes' theorem, the posterior probability density function (PDF) of $\boldsymbol{\theta}$ given by FFT data of output vibration satisfies

$$p(\boldsymbol{\theta}|\{\boldsymbol{Z}_k\}) \propto p(\boldsymbol{\theta}) p(\{\boldsymbol{Z}_k\}|\boldsymbol{\theta}) \tag{4}$$

where $p(\boldsymbol{\theta})$ is the prior PDF of $\boldsymbol{\theta}$. By assuming a non-informative prior distribution, the posterior PDF of $\boldsymbol{\theta}$ $p(\boldsymbol{\theta}|\{\boldsymbol{Z}_k\})$ is proportional to the likelihood function $p(\{\boldsymbol{Z}_k\}|\boldsymbol{\theta})$:

$$p(\boldsymbol{\theta}|\{\boldsymbol{Z}_k\}) \propto p(\{\boldsymbol{Z}_k\}|\boldsymbol{\theta}) = (2\pi)^{-(N_q-1)/2}\left[\prod_k \det \boldsymbol{C}_k(\boldsymbol{\theta})\right]^{-1/2} \times \exp\left[-(1/2)\sum_k \boldsymbol{Z}_k^T \boldsymbol{C}_k(\boldsymbol{\theta})^{-1}\boldsymbol{Z}_k\right] \tag{5}$$

For convenience, the log-likelihood function $L(\boldsymbol{\theta})$ is used:

$$p(\boldsymbol{\theta}|\{\boldsymbol{Z}_k\}) \propto \exp[-L(\boldsymbol{\theta})] \tag{6}$$

where $L(\boldsymbol{\theta}) = \frac{1}{2}\sum_k \ln\det \boldsymbol{C}_k(\boldsymbol{\theta}) + \frac{1}{2}\sum_k \boldsymbol{Z}_k^T \boldsymbol{C}_k(\boldsymbol{\theta})^{-1}\boldsymbol{Z}_k$. Minimizing $L(\boldsymbol{\theta})$, which is equivalent to maximizing $p(\boldsymbol{\theta}|\{\boldsymbol{Z}_k\})$, one can obtain the most probable values of the modal parameters $\boldsymbol{\theta}$. A factor

$$\gamma_k = \mathrm{Re}\boldsymbol{H}_k / S_e^2 \tag{7}$$

is introduced, which is a ratio of the modal spectral density of displacement response to the square of prediction error. It is natural to refer to γ_k as the signal-to-noise ratio at the frequency f_k.

2.2. 3D-DIC

3D-DIC combines a stereo-vision technique, the triangulation method, and DIC. Two-dimensional DIC originally developed in the early 1980s needs a series of images of a specimen before and after deformation [12,32]. The surface of a specimen requires a random speckle pattern on it. By selecting one of the images in the series as a reference image and dividing it into subsets, a correlation algorithm is used on each subset to identify corresponding subsets in all the other images of the series. The corresponding subsets are matched by finding peaks of the cross-correlation function or any other correlation metric. The displacement vector is defined by the reference subset and its matched subset in another image so that the displacement distribution map is obtained.

In 3D-DIC, two cameras need to capture a pair of images of the specimen surface that has random speckles on it. The procedure of 3D-DIC measurement is shown in Fig. 1. With the stereo-vision technique and triangulation method, 3D information in the global coordinate system (GCS) with axes (X, Y, Z) is recovered by the two cameras. The cross-correlation function is calculated twice: first to identify (X, Y, Z) coordinates of each subset in the pair of images and second to match them with those of the corresponding subsets in deformed images. As a result, 3D-DIC gives (X, Y, Z) coordinates of the specimen of each pair of images before and after deformation. Displacements are easily calculated from the coordinates. With the full-field displacement, one can select as many DOFs of the specimen as possible for vibration measurement, which resolves the drawback of a small number of sensors in the traditional pointwise measurement method and has potential for local damage detection.

2.2.1. Modal identification of membranes by BOMA and 3D-DIC

Membranes are widely used in aerospace applications, and their dynamic characteristics have received extensive attention. However, it is difficult to obtain modal parameters of membranes by accelerometers due to light weight of materials of membranes and additional masses of the accelerometers. Thus, non-contact test methods have an important role in dynamic testing of membranes. Use of scanning laser Doppler vibrometry in the standard step-scan mode in modal measurement needs to scan a structure point by point, which will greatly increase the time required in the experimental process. For continuous scanning, since laser measures displacements of different locations at different times, advanced signal processing methods are needed to extract operational deflection shapes of a structure. In addition, since sinusoidal excitation is usually used for scanning laser vibrometry and random excitation may not be used there, it is difficult to apply BOMA in scanning

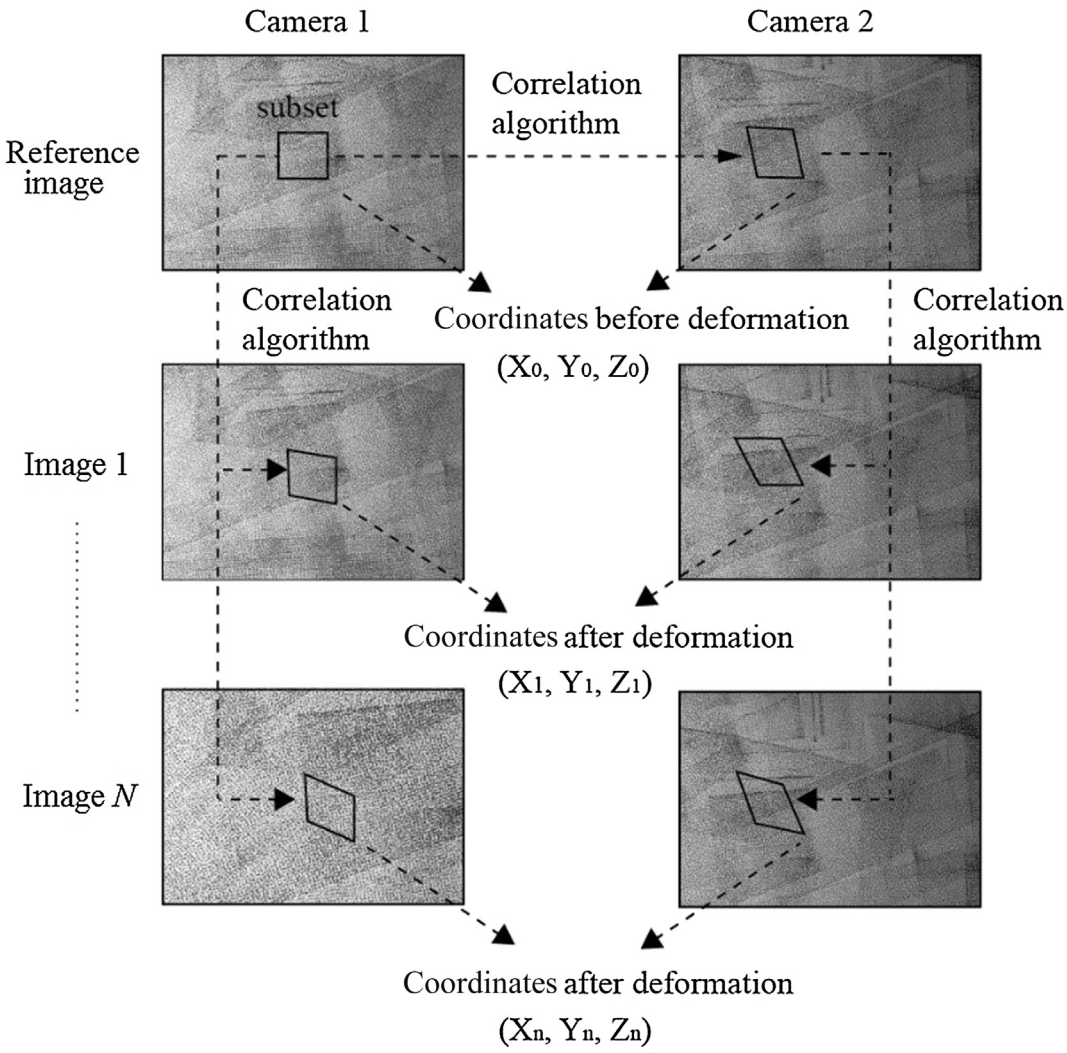

Fig. 1. Procedure of 3D-DIC measurement, where the subscripts 0, 1, . . . , n denote undeformed and subsets of deformed images.

laser vibrometry in modal measurement. Also, due to small stiffness of a membrane, deformation of a membrane can be relatively large and scanning laser Doppler vibrometry can yield relatively large error. Therefore, the 3D-DIC full-field dynamic test combined with the BOMA modal identification method has great advantages in identification of modal parameters of membranes because such a method only requires one set of response time histories. In this work, 3D-DIC is applied to record displacements of damaged membranes. By using such a non-contact method, one can obtain more vibration data compared with the traditional pointwise measurement method, and no mass loading of sensors is incurred on a membrane. Such a method brings possibilities for detecting local damage in a structure based on dynamic measurement. Moreover, accurate mode shapes are obtained through BOMA, which resolves drawbacks that input excitation data need to be recorded and post-processed in normal 3D-DIC dynamic measurement, such as EMA. High efficiency of the method is mainly reflected in its experimental process. An entire experiment can generally be completed within a few minutes. When photo images are obtained, displacement responses can be extracted off-line by a computer without human participation. In the following section, two indices are used to detect and quantify damage by using accurate mode shapes of the membrane: one index uses mean curvature mode shapes, and the other index is the MSDI that is used to improve local damage detection of the membrane.

3. Experimental local damage detection

Two membranes with a random speckle pattern sprayed on one surface of each membrane were used in experiment. One was an 11 cm radius circular membrane whose boundary is fixed on a circular ring with a double-faced adhesive tape, which may not be an ideally fixed boundary, and the other was a rectangular membrane of 22 cm $\times$ 31 cm with fixed upper and right sides, which may not be ideally fixed either. A thin razor cut of approximately 7 mm long was made in the circular membrane to represent its local damage and a thin razor cut of approximately 19 mm long was made in the rectangular membrane, as shown in Fig. 2.

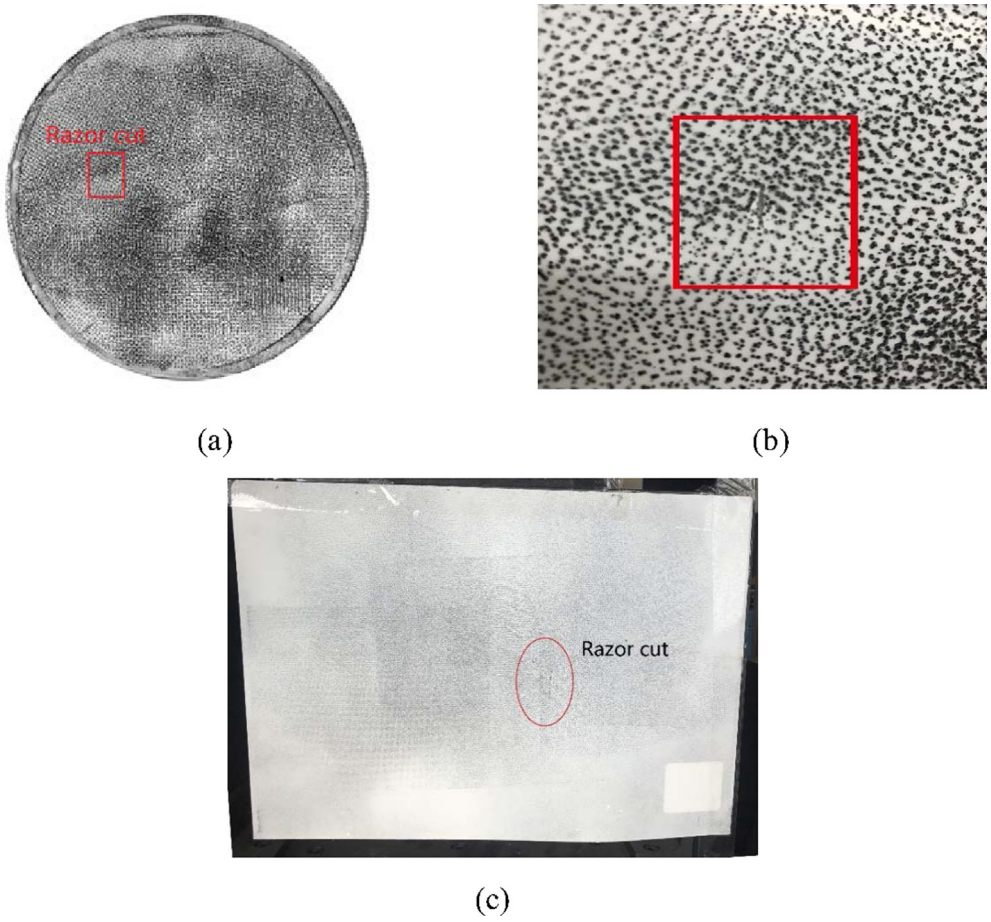

Fig. 2. (a) Circular membrane with a razor cut, (b) a detailed view of the razor cut on the circular membrane, and (c) a rectangular membrane with a razor cut.

Modal parameters of the circular membrane fixed on its boundary under ambient excitation were first extracted. In order to detect local damage in the circular membrane, dense measurement points were applied to it. The purpose of this example is to verify that global mode shapes of a structure can be correctly extracted since global mode shapes of a circular membrane are well known, and to verify that local damage detection can be achieved by the proposed method with enough measurement points in a structure. Further, results of the rectangular membrane with different boundary conditions and global mode shape measurement demonstrate feasibility of the method for local damage detection.

One surface on each membrane was first painted with white and black dots that were randomly sprayed on it. Sizes of black dots were controlled to match with camera resolution. A loud speaker behind a membrane was used to generate a random signal, which simulated ambient excitation, to excite the membrane. Two Photron high-speed cameras, each with resolution of up to 1280 $\times$ 1024 pixels, and a Nikon lens (AF 28 mm/2.8D) were used to capture images at a frame rate of 800f/s, which is sufficient to analyze the first few natural frequencies of the membranes. The experimental setup for the circular membrane is shown in Fig. 3. Two cameras were located in front of a membrane, and each camera has a certain angle with respect to the membrane. Angles of the cameras can be obtained from the stereo-vision technique and triangulation method. In the current work, the angles are about 45 degrees. The measurement distance is important for testing results, which is related to pixels of the cameras, sizes of speckles, focal lengths of lenses of the cameras and so on. One of the most basic guidelines is to ensure that there are three to five pixels in each speckle. By taking the above factors into account, the measurement distance in the current work is about 800 mm. The BOMA method can be used under ambient excitation that can be described as random white noise. Since environmental excitation in the lab is very weak, in order to obtain good identified

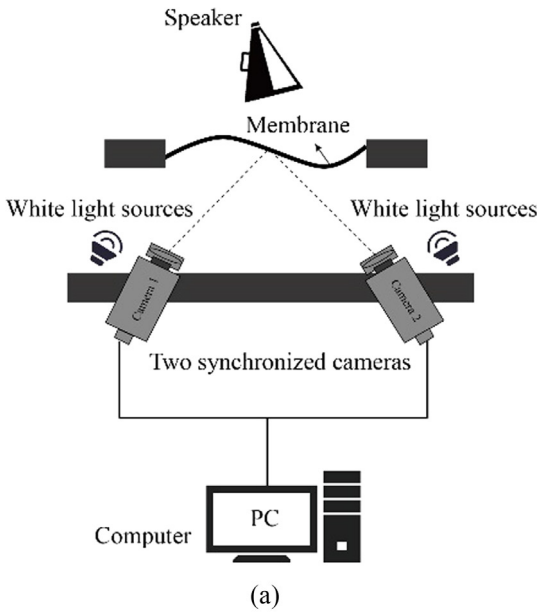

Fig. 3. (a) Schematic and (b) the photo of the experimental setup for vibration measurement of the circular membrane based on 3D-DIC.

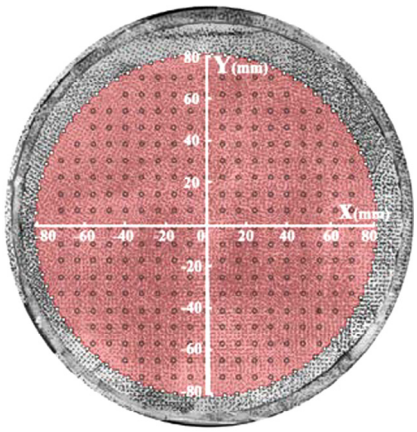

Fig. 4. Analyzed area of the circular membrane with 301 measurement points.

results, random white noise excitation from a speaker is used for damage detection. BOMA does not require specific knowledge of excitation. A speaker is used here to generate random white noise to simulate loading on the membranes without recording it. Moreover, it is easy and economical to use a speaker in the experiment. Applying a speaker to generate white noise to simulate ambient loading is well suited for membranes. In fact, random white noise from a speaker is often used in damage detection with use of OMA [11]. When the speaker started to excite a membrane, the two high-speed cameras could synchronously capture deformed speckle images. A commercial 3D-DIC algorithm is used to analyze each pair of images of the two cameras to obtain the 3D full-field displacement of the membrane.

3.1. Local damage detection by a mean curvature mode shape

In order to validate the proposed method, mode shapes of the circular membrane were first obtained by the BOMA method. An analyzed area of the circular membrane was a circle with an approximate diameter of 72 mm, as shown in

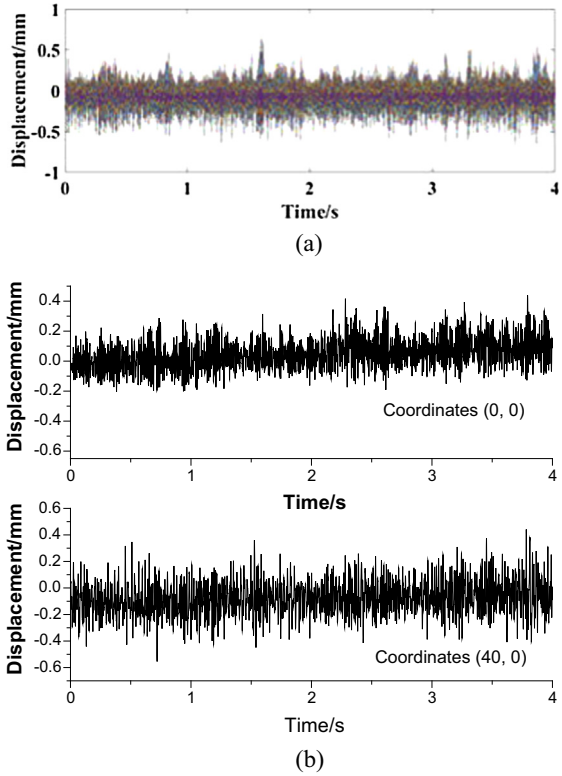

Fig. 5. (a) Time history curves of displacements of all the measurement points of the circular membrane, and (b) time history curves of displacements at coordinates (0, 0) and (40, 0) of the membrane.

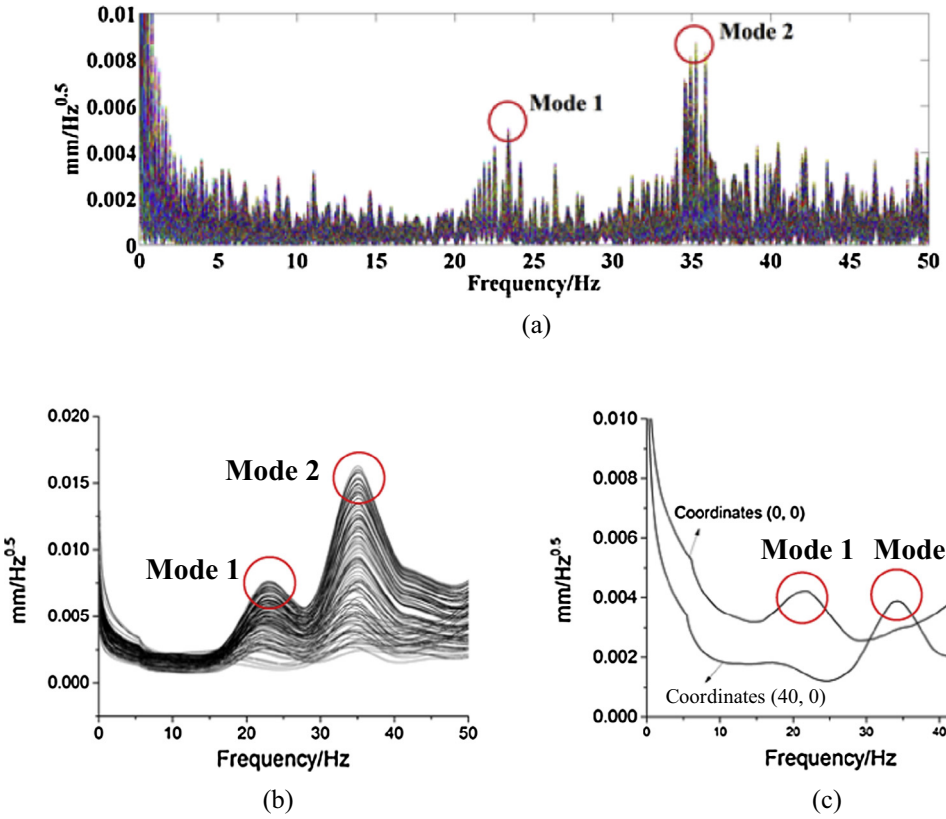

Fig. 6. (a) PSDs and (b) singular-value spectra of all the measurement points of the circular membrane, and (c) singular-value spectra of the measurement points with coordinates (0, 0) and (40, 0).

Table 1
Identified modal parameters of the circular membrane.

Mode	f (Hz)	ζ (%)	S (10^{-5} mm^2/Hz)	S_e (10^{-6} mm^2/Hz)	γ
1	22.86	0.042	4.23	1.06	5037.51
2	35.48	0.044	10.1	5.08	3265.89

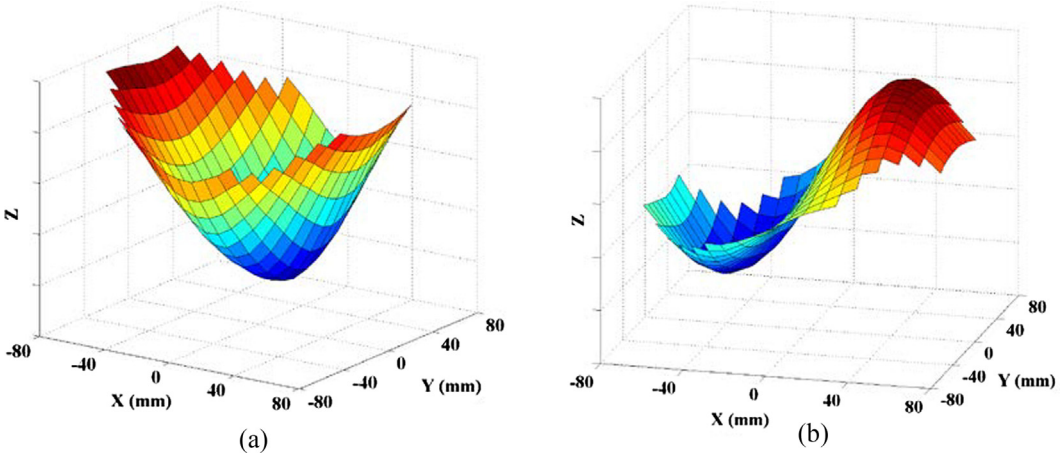

Fig. 7. (a) First mode shape of the circular membrane and (b) its second mode shape.

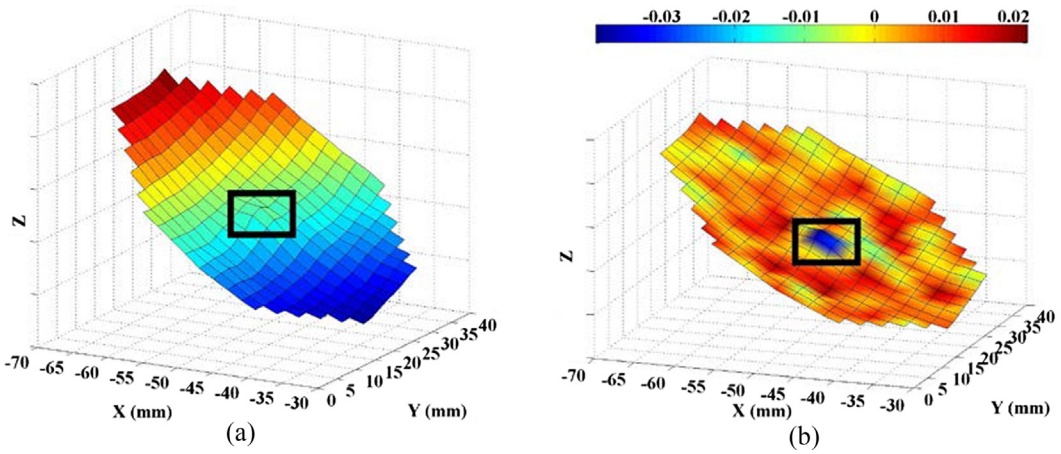

Fig. 8. (a) First local mode shape of the circular membrane and (b) its first local mean curvature mode shape.

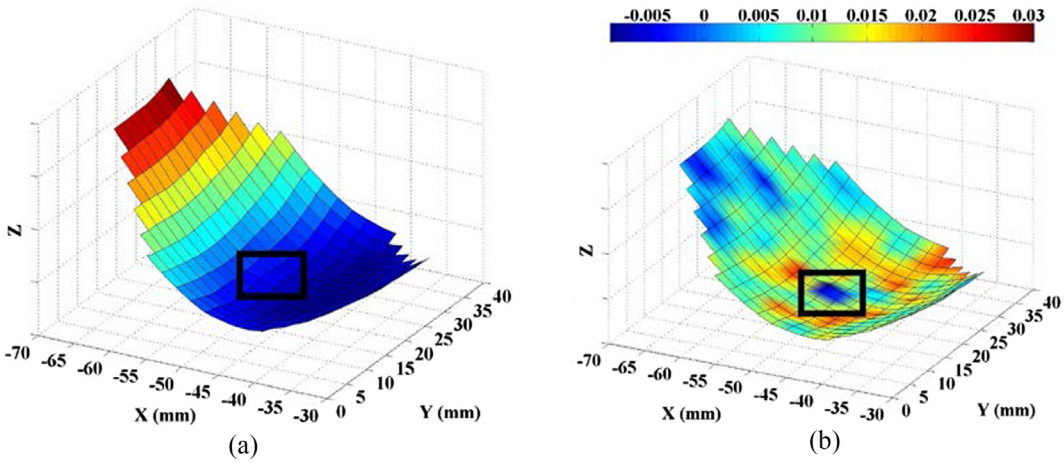

Fig. 9. (a) Second local mode shape of the circular membrane and (b) its second local mean curvature mode shape.

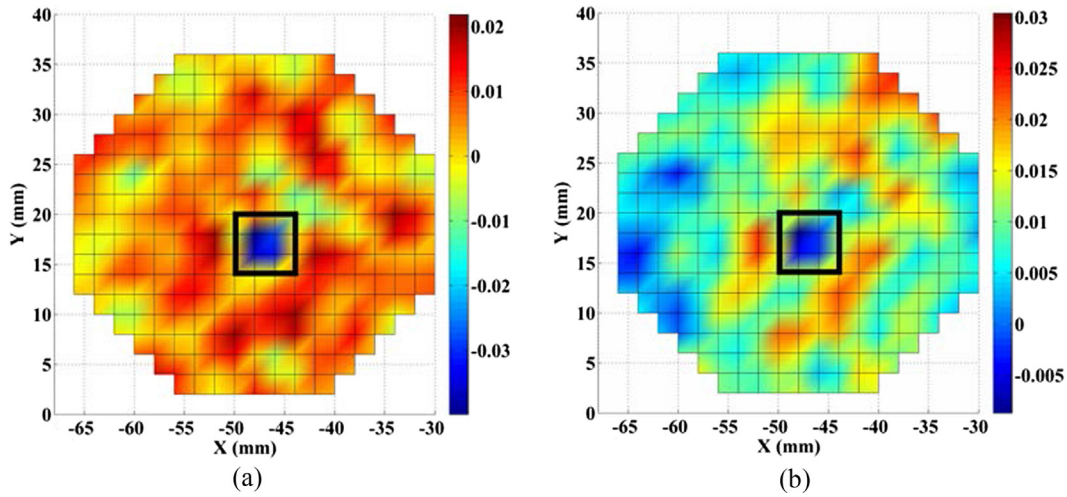

Fig. 10. X-Y views of the (a) first and (b) second local mean curvature mode shapes of the circular membrane.

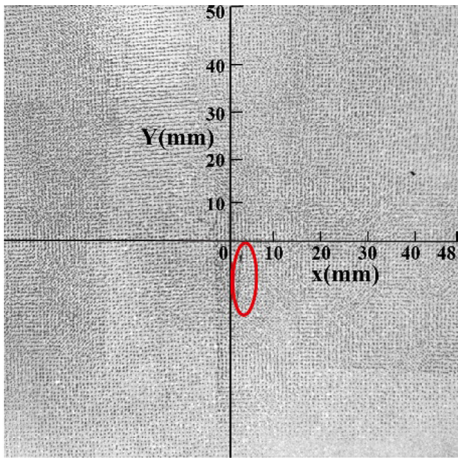

Fig. 11. Analyzed area of the rectangular membrane.

Fig. 4, and there were 301 measurement points on it. Fig. 5(a) and (b) show time history curves of displacements of all the measurement points of the circular membrane and two points with coordinates (0, 0) and (40, 0) on it, respectively. The power of the speaker is small enough so as not to increase its damage; the maximum displacement of the membrane is smaller than 0.5 mm.

Fig. 6(a) and (b) show PSDs and singular-value spectra of different measurement points of the circular membrane, respectively. It is difficult to select peaks from PSDs due to inappropriately scaled abscissa. Thus, singular-value spectra are given from FFT results. The peaks can be easily selected with singular-value spectra, where two peaks can be obviously seen near 23 Hz and 35 Hz in the 0–50 Hz range. Two frequency ranges such as 20–25 Hz and 30–40 Hz were then used to identify modal parameters of the circular membrane by BOMA. In addition, a measurement point that is close to the maximum amplitude point of a mode shape is sensitive to the corresponding natural frequency, and the singular-value spectrum of the measurement point has a sharp peak at the corresponding natural frequency, as shown in Fig. 6(b) and (c). A measurement point that is close to the minimum amplitude point of a mode shape is insensitive to the corresponding natural frequency, and the singular-value spectrum is smooth at the corresponding natural frequency, as shown in Fig. 6(b) and (c). Table 1 gives its identified modal parameters of the first two orders. Fig. 7 shows that the first two global mode shapes of the membrane, which are consistent with what one expects for a circular membrane. It can be seen from Fig. 6(c) and Fig. 7 that the center measurement point of the circular membrane with coordinates (0, 0) and another measurement point

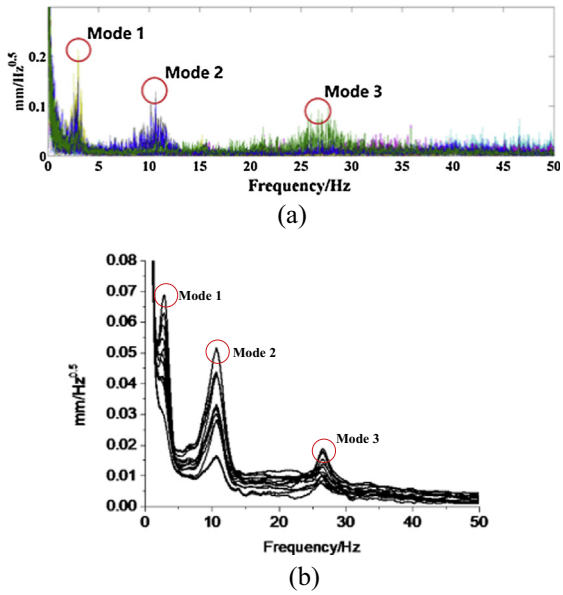

Fig. 12. (a) PSDs and (b) singular-value spectra of different measurement points of the rectangular membrane.

Table 2
Identified modal parameters of the rectangular membrane.

Mode	f (Hz)	ζ (%)	S (mm^2/Hz)	S_e (10^{-5}mm^2/Hz)	γ
1	3.21	0.059	0.12	15.7	54079.64
2	10.61	0.105	0.019	6.39	7004.92
3	27.27	0.027	0.007	3.71	62993.3

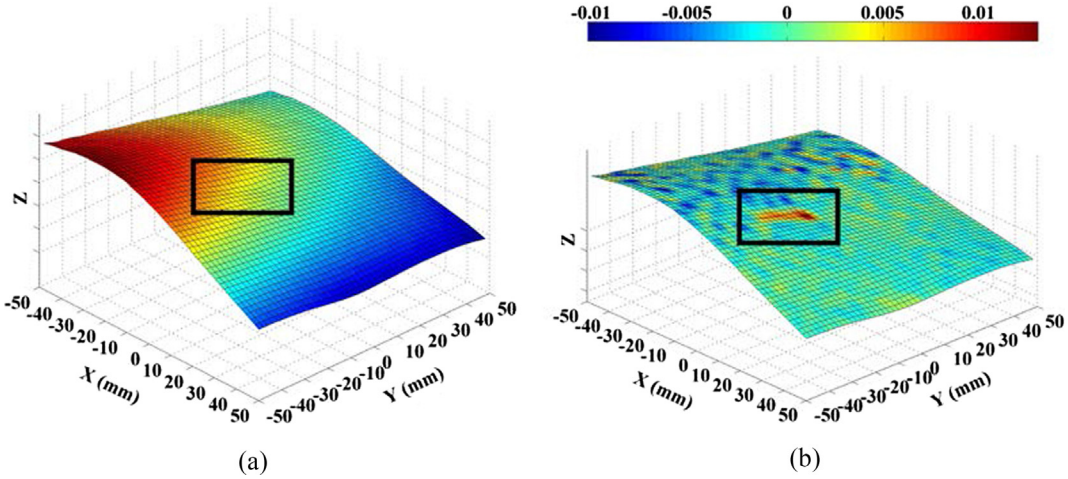

Fig. 13. (a) First global mode shape of the rectangular membrane and (b) its first global mean curvature mode shape.

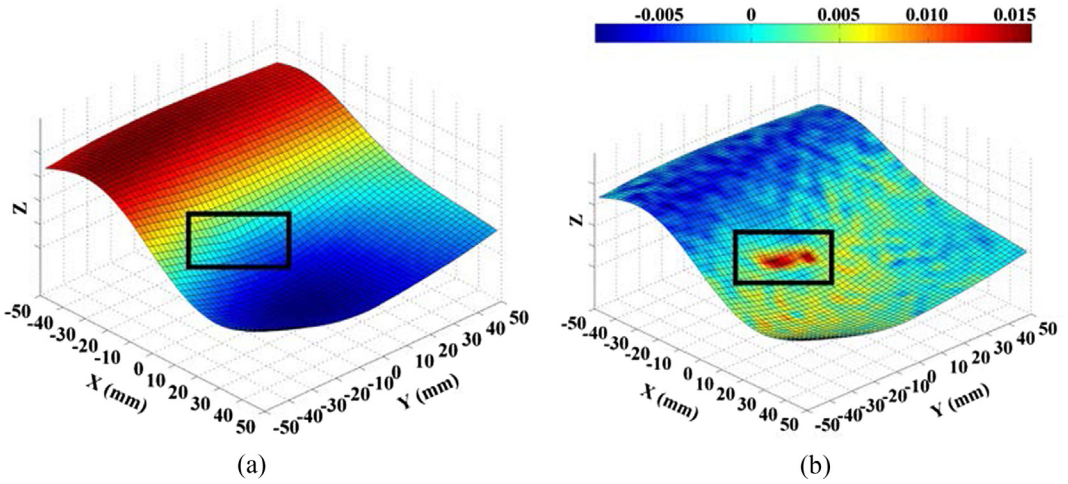

Fig. 14. (a) Second global mode shape of the rectangular membrane and (b) its second global mean curvature mode shape.

with coordinates (40, 0) are close to the minimum amplitude points of the second and first mode shapes, respectively; singular-value spectra of the two measurement points are smooth at the second and first natural frequencies, respectively. With 301 measurement points in the analyzed area, the global mode shapes in Fig. 7 are smooth and the damage area cannot be observed. This is due to the fact that horizontal and vertical distances of neighboring measurement points are 8 mm, whereas the razor cut is only 7 mm long. Due to this reason, denser measurement points were needed to detect the local damage. Another analyzed area was chosen, which was a circle centered around the center of the damage with an approximate diameter of 18 mm, and there were 301 measurement points in the analyzed area; horizontal and vertical distances between neighboring measurement points are 2 mm. Figs. 8 and 9 depict the first two local mode shapes of the membrane and its first two local mean curvature mode shapes [16]. Fig. 10 depicts X-Y views of the first two local mode mean curvature mode shapes.

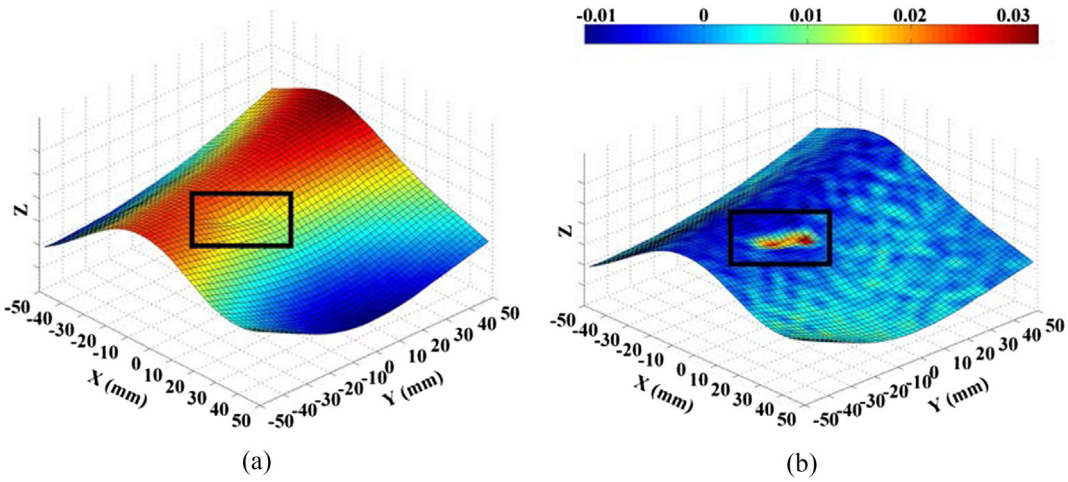

Fig. 15. (a) Third global mode shape of the rectangular membrane and (b) its third global mean curvature mode shape.

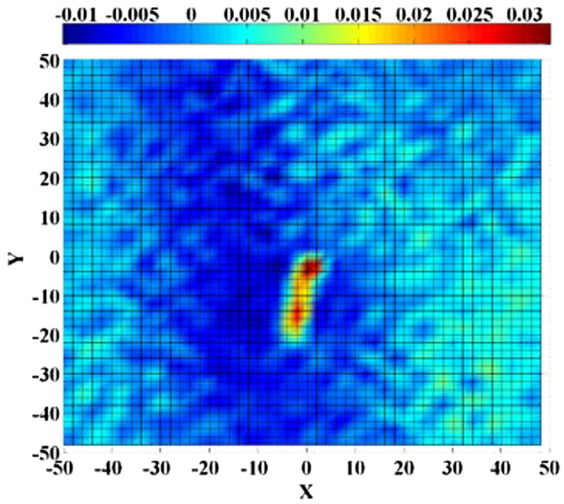

Fig. 16. X-Y view of the third global mean curvature mode shape of the rectangular membrane.

The anomaly area displayed in the first local mode shape of the circular membrane is at the center of the analyzed area, where the razor cut is. Moreover, the first local mean curvature mode shape more clearly identifies the damage location. Anomaly also exits in the second local mode shape and second local mean curvature mode shape. Anomaly or the damage area occurs near anti-nodes of the first or second local mean curvature mode shape of the membrane. The above results show that there are anomalies in the local mode shapes or local mean curvature mode shapes at the damage location. The damage location can be identified by the local mode shapes and local curvature mode shapes.

Another experiment was conducted on the rectangular membrane. An analyzed area of the membrane was a rectangle of 98 mm $\times$ 98 mm, as shown in Fig. 11, and there were 50 $\times$ 50 measurement points. Fig. 12(a) and (b) shows PSDs and singular-value spectra at different measurement points of the rectangular membrane, respectively, where three peaks can be obviously seen near 3 Hz, 10 Hz, and 27 Hz within 0–50 Hz. Three frequency ranges such as 1–5 Hz, 6–14 Hz, and 20–30 Hz are then used to identify modal parameters of the rectangular membrane by BOMA. Table 2 gives its modal parameters of the first three orders. Global mode shapes of the membrane relative to its initial shape are fitted using coordinates of the 2500 measurement points from its initial reference image. Figs. 13–15 show the first three global mode shapes of the membrane and its first three global mean curvature mode shapes. Fig. 16 shows the X-Y view of the third global mean curvature mode shape.

The damage area is less prominent from the first and second mode shapes than the third mode shape from which anomaly in the analyzed area can be clearly seen. Anomaly is more clearly seen in each of the three global mean curvature mode

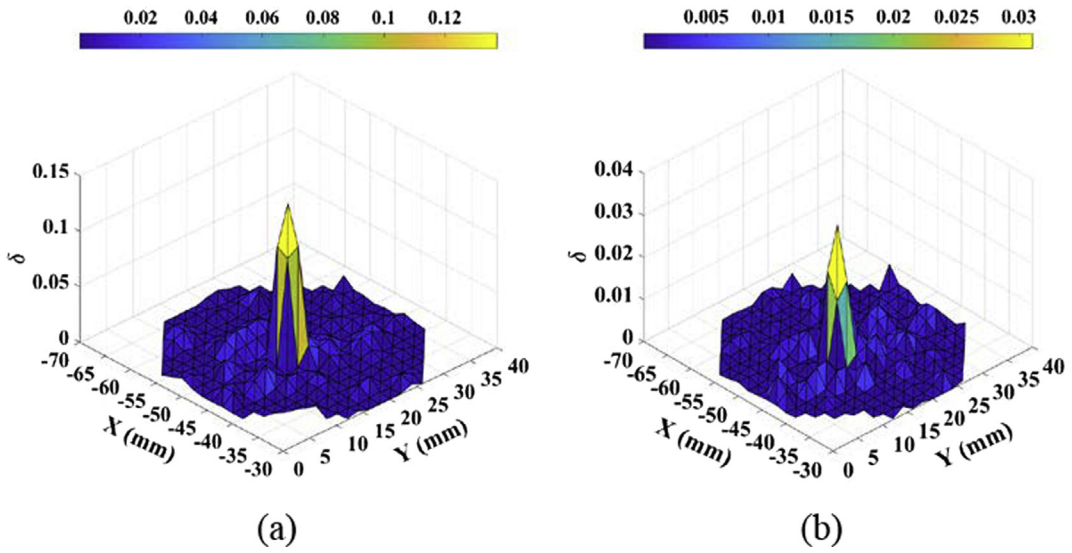

Fig. 17. MSDIs δ associated with the (a) first and (b) second local mode shapes of the circular membrane.

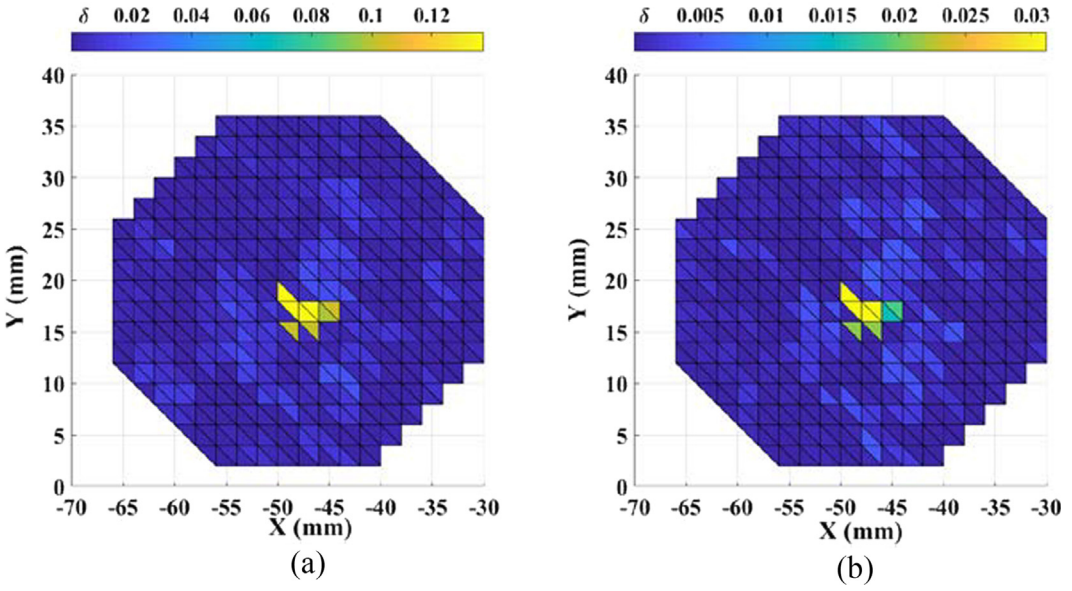

Fig. 18. X-Y views of δ associated with the (a) first and (b) second local mode shapes of the circular membrane.

shapes than each of the three global mode shapes, respectively, which identifies the damage location. The anomaly area in Fig. 16 is in good agreement with the actual location of the cut in Fig. 11.

3.2. Local damage detection by the MSDI

A point $\boldsymbol{p}$ on a two-dimensional undeformed flat membrane can be described by coordinates x and y, and its mode shape $\boldsymbol{Z}$ can be expressed as a function of x and y:

$$\boldsymbol{Z}(\boldsymbol{p}) = \boldsymbol{Z}(x, y) \tag{8}$$

The MSDI is defined by [31]

$$\delta(\boldsymbol{p}) = \left[\boldsymbol{Z}^d(\boldsymbol{p}) - \boldsymbol{Z}^p(\boldsymbol{p})\right]^2 \tag{9}$$

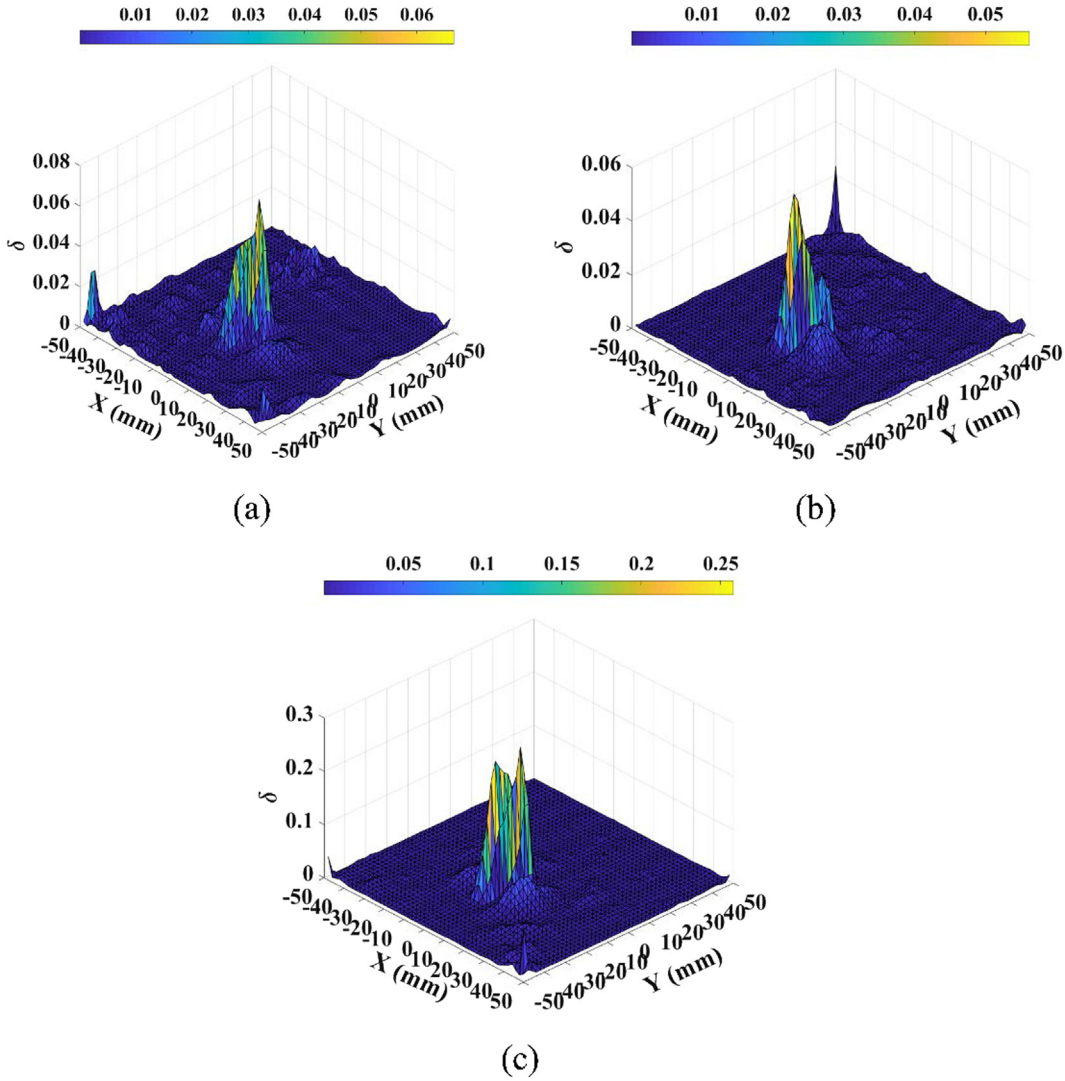

Fig. 19. MSDIs associated with the (a) first, (b) second, and (c) third global mode shapes of the rectangular membrane.

where $\boldsymbol{Z}^d$ is a mode shape of a damaged membrane and $\boldsymbol{Z}^p$ is the corresponding mode shape from a polynomial that fits $\boldsymbol{Z}^d$ with a properly determined order; $\boldsymbol{Z}^p$ can be considered as the mode shape of the associated undamaged membrane. Note that both $\boldsymbol{Z}^d$ and $\boldsymbol{Z}^p$ are in vector forms. The MSDI is used to further assist local damage detection, and structural damage can be identified in neighborhoods with high values of the MSDIs.

The mode shape $\boldsymbol{Z}^p$ at $\mathbf{p}$ from a polynomial fit with an order n can be expressed by

$$\boldsymbol{Z}^p(\boldsymbol{p}) = \boldsymbol{Z}^p(x,y) = \sum_{k=0}^{n}\sum_{i=0}^{k} a_{i,k-i}x^i y^{k-i} \tag{10}$$

where $a_{i,k-i}$ are coefficients of the polynomial that fits $\boldsymbol{Z}^d$. Note that increasing n can improve the level of approximation of $\boldsymbol{Z}^p$ to $\boldsymbol{Z}^d$. A fitting index fit and a convergence index con in Ref. [31] are used to determine a proper value of n so that anomaly caused by damage on a membrane can be retained and manifested in δ. The fitting index fit that is defined by

$$\mathrm{fit}(n) = \frac{\mathrm{RMS}(\boldsymbol{Z}^d)}{\mathrm{RMS}(\boldsymbol{Z}^d) + \mathrm{RMS}(\boldsymbol{e})} \times 100\% \tag{11}$$

where $\mathrm{RMS}(\cdot)$ denotes the root-mean-square value of a vector and $\boldsymbol{e} = \boldsymbol{Z}^d - \boldsymbol{Z}^p$ is an error vector with the polynomial order n, can quantify the level of approximation of $\boldsymbol{Z}^p$ to $\boldsymbol{Z}^d$. The convergence index con can be expressed by

$$\mathrm{con}(n) = \mathrm{fit}(n) - \mathrm{fit}(n-2) \tag{12}$$

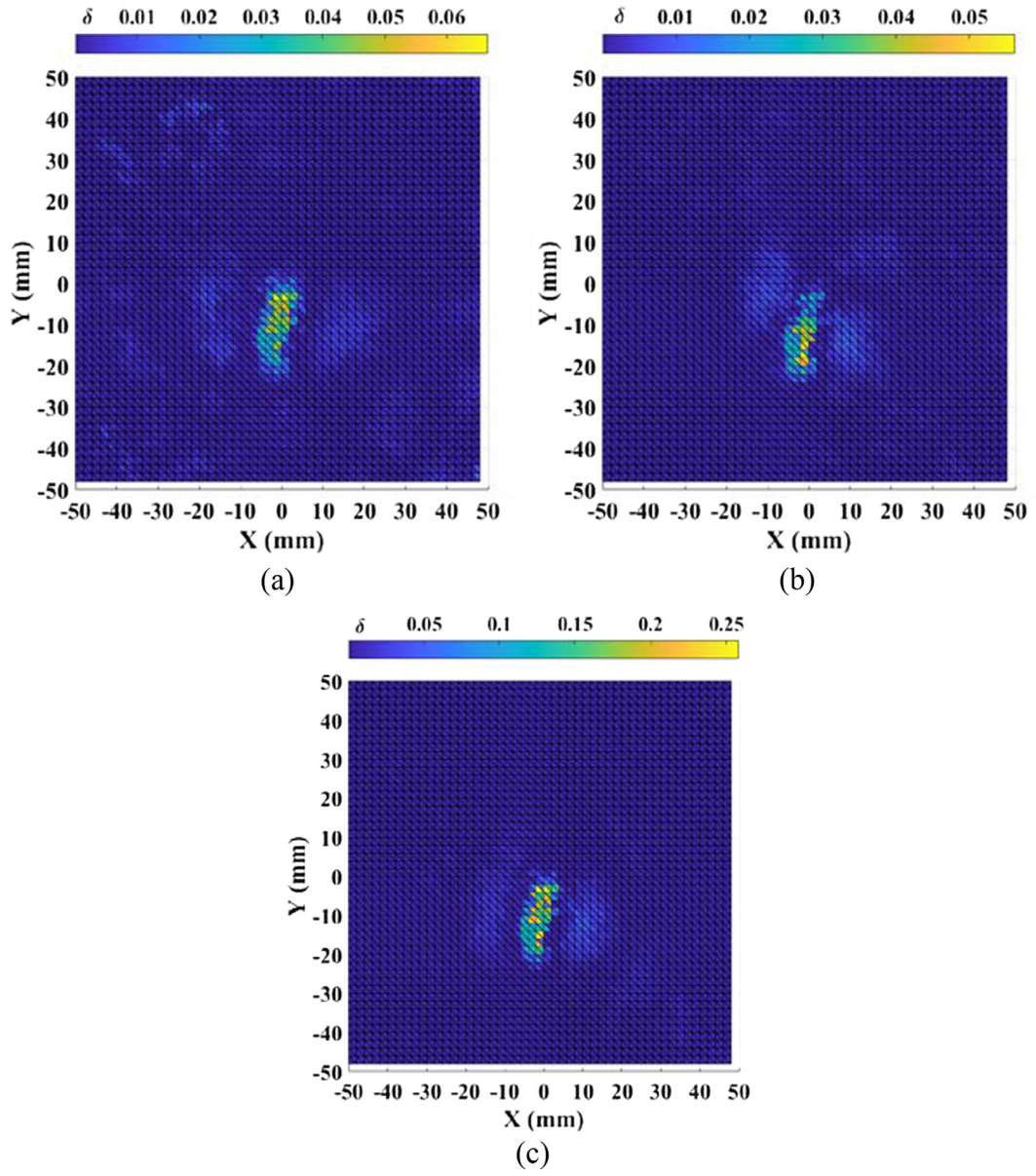

Fig. 20. X-Y views of δ associated with the (a) first, (b) second, and (c) third global mode shapes of the rectangular membrane.

The proper value of n can be obtained by increasing its value and calculating con in Eq. (12). The proper value of n is the smallest one with which con is smaller than a threshold value, which is con $= 0.5\%$ in this work.

MSDIs δ and their X-Y views associated with the first and second local mode shapes of the circular membrane are shown in Figs. 17 and 18, respectively. The cut in the circular membrane can be clearly identified in neighborhoods with high values of δ. MSDIs δ associated with the first, second, and third global mode shapes of the rectangular membrane are shown in Fig. 19(a)–(c), respectively. It can be found that the cut in the rectangular membrane corresponds to high values of δ. However, there are high values of δ at some corners of the rectangular membrane. They are caused by the polynomial fit at some corners of the rectangular membrane; X-Y views of δ without values at some corners of the rectangular membrane are shown in Fig. 20(a)–(c). The cut in the rectangular membrane can be clearly identified.

4. Conclusions

A novel method that combines BOMA and 3D-DIC is proposed to detect local damage in circular and rectangular membranes with razor cuts and different boundary conditions under ambient excitation. Main advantages of the method are that it is a noncontact and full-field vibration measurement method that can detect local damage of a structure under ambient

excitation without any added mass on the structure, and boundary conditions of the structure can be non-ideal. Since the method only requires ambient excitation, input excitation data are not needed. When local damage is present, it manifests itself as anomaly in a local or global mode shape or a local or global curvature mode shape with good visibility. The method can be easily implemented. It can provide quantitative information on the amplitude of vibration of a structure and overcome disadvantages of the technique in Ref. [11]. Using MSDIs can further improve local damage detection results. Use of the first two or three mode shapes of the membranes can identify locations of their local damage, and the identified locations of the local damage from the first two or three mode shapes are consistent.

Acknowledgement

The authors would like to thank the financial support from the Shanghai Natural Science Foundation (Project No. 17ZR1419800), the Shanghai Science and Technology Innovation Fund (Project No. 17060502600), and the National Science Foundation (Award Nos. 1335024, 1763024, and 1762917).

References

[1] P. Cawley, R.D. Adams, The location of defects in structures from measurements of natural frequencies, J. Strain Anal. Eng. Des. 14 (1979) 49–57, https://doi.org/10.1243/03093247V142049.
[2] A.K. Pandey, M. Biswas, M.M. Samman, Damage detection from changes in curvature mode shapes, J. Sound Vib. 145 (1991) 321–332, https://doi.org/10.1016/0022-460X(91)90595-B.
[3] C.P. Ratcliffe, Damage detection using a modified laplacian operator on mode shape data, J. Sound Vib. 204 (1997) 505–517, https://doi.org/10.1006/jsvi.1997.0961.
[4] J.T. Kim, N. Stubbs, Damage detection in offshore jacket structures from limited modal information, Int. J. Offshore Polar Eng. 5 (1995) 58–66.
[5] G. Pedrini, W. Osten, M.E. Gusev, High-speed digital holographic interferometry for vibration measurement, Appl. Opt. 45 (2006) 3456, https://doi.org/10.1364/AO.45.003456.
[6] C. Papadimitriou, D.C. Papadioti, Component mode synthesis techniques for finite element model updating, Comput. Struct. 126 (2013) 15–28.
[7] F.L. Zhang, Y.C. Ni, H.F. Lam, Bayesian structural model updating using ambient vibration data collected by multiple setups, Struct. Control Health Monit. 24 (12) (2017), https://doi.org/10.1002/stc.2023 e2023.
[8] H.A. Jensen, C. Esse, V. Araya, et al, Implementation of an adaptive meta-model for bayesian finite element model updating in time domain, Reliab. Eng. Syst. Saf. 160 (2016) 174–190.
[9] F.-P. Chiang, R.-M. Juang, Laser speckle interferometry for plate bending problems, Appl. Opt. 15 (1976), https://doi.org/10.1364/AO.15.002199.
[10] F.-P. Chiang, Q.B. Li, Real-time laser speckle photography, Appl. Opt. 23 (1984) 4469–4470.
[11] L. Keene, F.P. Chiang, Real-time anti-node visualization of vibrating distributed systems in noisy environments using defocused laser speckle contrast analysis, J. Sound Vib. 320 (2009) 472–481, https://doi.org/10.1016/j.jsv.2008.08.022.
[12] W.H. Peters, W.F. Ranson, Digital imaging techniques in experimental stress analysis, Opt. Eng. 21 (1982), https://doi.org/10.1117/12.7972925.
[13] M. Sutton, W. Wolters, W. Peters, W. Ranson, S. McNeill, Determination of displacements using an improved digital correlation method, Image Vis. Comput. 1 (1983) 133–139, https://doi.org/10.1016/0262-8856(83)90064-1.
[14] P.-C. Hung, A.S. Voloshin, In-plane strain measurement by digital image correlation, J. Brazilian Soc. Mech. Sci. Eng. 25 (2003) 215–221, https://doi.org/10.1590/S1678-58782003000300001.
[15] P. Avitabile, J. Baqersad, C. Niezrecki, Using digital image correlation and three dimensional point tracking in conjunction with real time operating data expansion techniques to predict full-field dynamic strain, AIP Conf. Proc. (2014) 3–22, https://doi.org/10.1063/1.4879564.
[16] G. Machado, D. Favier, G. Chagnon, Membrane curvatures and stress-strain full fields of axisymmetric bulge tests from 3D-DIC measurements. Theory and validation on virtual and experimental results, Exp. Mech. 52 (2012) 865–880, https://doi.org/10.1007/s11340-011-9571-3.
[17] M.N. Helfrick, C. Niezrecki, P. Avitabile, T. Schmidt, 3D digital image correlation methods for full-field vibration measurement, Mech. Syst. Signal Process. 25 (2011) 917–927, https://doi.org/10.1016/j.ymssp.2010.08.013.
[18] P.L. Reu, D.P. Rohe, L.D. Jacobs, Comparison of DIC and LDV for practical vibration and modal measurements, Mech. Syst. Signal Process. 86 (2017) 2–16, https://doi.org/10.1016/j.ymssp.2016.02.006.
[19] T.J. Beberniss, D.A. Ehrhardt, High-speed 3D digital image correlation vibration measurement: recent advancements and noted limitations, Mech. Syst. Signal Process. 86 (2017) 35–48, https://doi.org/10.1016/j.ymssp.2016.04.014.
[20] M. Hagara, F. Trebuňa, R. Huňady, M. Kalina, M. Schrötter, Experimental identification of modal parameters of thin metal sheets by using of DIC, Procedia Eng. 48 (2012) 180–188, https://doi.org/10.1016/j.proeng.2012.09.503.
[21] A. Zanarini, Broad frequency band full field measurements for advanced applications: point-wise comparisons between optical technologies, Mech. Syst. Signal Process. 98 (2018) 968–999, https://doi.org/10.1016/j.ymssp.2017.05.035.
[22] P. Poozesh, J. Baqersad, C. Niezrecki, P. Avitabile, A multi-camera stereo DIC system for extracting operating mode shapes of large scale structures, Conf. Proc. Soc. Exp. Mech. Ser. (2016) 225–238, https://doi.org/10.1007/978-3-319-22446-6_29.
[23] P. Poozesh, A. Sarrafi, Z. Mao, C. Niezrecki, Modal parameter estimation from optically-measured data using a hybrid output-only system identification method, Measurement 110 (2017) 134–145, https://doi.org/10.1016/j.measurement.2017.06.030.
[24] K.V. Yuen, L.S. Katafygiotis, Bayesian time-domain approach for modal updating using ambient data, Probabilistic Eng. Mech. 16 (2001) 219–231, https://doi.org/10.1016/S0266-8920(01)00004-2.
[25] K. Yuen, L. Katafygiotis, Bayesian fast Fourier transform approach for modal updating using ambient data, Adv. Struct. Eng. 6 (2003) 81–95, https://doi.org/10.1260/136943303769013183.
[26] S.-K. Au, F.-L. Zhang, Y.-C. Ni, Bayesian operational modal analysis: theory, computation, practice, Comput. Struct. 126 (2013) 3–14, https://doi.org/10.1016/j.compstruc.2012.12.015.
[27] P. Liu, P.Y. Lian, W.G. Yang, Horizontal resonance of a 13 story building under external machine vibrations, Int. J. Struct. Stab. Dyn. 18 (2018) 1850005.
[28] Y.C. Ni, X.L. Lu, W.S. Lu, Operational modal analysis of a high-rise multi-function building with dampers by a Bayesian approach, Mech. Syst. Sig. Process. 86 (2017) 286–307.
[29] F.L. Zhang, C.E. Ventura, H.B. Xiong, et al, Evaluation of the dynamic characteristics of a super tall building using data from ambient vibration and shake table tests by a Bayesian approach, Struct. Control Health Monit. 25 (2018), https://doi.org/10.1002/stc.2121 e2121.
[30] S.-K. Au, Fast bayesian FFT method for ambient modal identification with separated modes, J. Eng. Mech. 137 (2011) 214–226, https://doi.org/10.1061/(ASCE)EM.1943-7889.0000213.
[31] Y. Xu, W. Zhu, Non-model-based damage identification of plates using measured mode shapes, Struct. Heal. Monit. 16 (2017) 3–23, https://doi.org/10.1177/1475921716655974.
[32] I. Yamaguchi, Speckle displacement and decorrelation in the diffraction and image fields for small object deformation, Opt. Acta (Lond) 28 (1981) 1359–1376, https://doi.org/10.1080/713820454.